CrossMark

TECHNICAL ARTICLE

Relations of Chemical Composition to Solidification Behavior and Associated Microstructure of Stellite Alloys

R. Liu[1,2] · J. H. Yao[2] · Q. L. Zhang[2] · M. X. Yao[3] · R. Collier[3]

Abstract Stellite alloys are a family of superalloys, which can be categorized as CoCrW and CoCrMo systems. Ten selected Stellite alloys from these systems, with low carbon or high carbon content, are studied with respect to solidification and microstructure using differential scanning calorimetry (DSC), scanning electron microscopy with an energy dispersive x-ray spectroscopy, and x-ray diffraction. The objective of this work is to investigate the effects of carton content and other alloying elements on the solidification behavior and associated microstructure of Stellite alloys, to provide the materials industry with technical guidance in design, manufacturing, processing, and heat treatment of these alloys. The phase transformation temperatures of these alloys during heating and cooling are determined under the DSC test. The solidified microstructures and the phases present are analyzed and discussed with emphasis on the relation to chemical composition.

Keywords Stellite alloy · Microstructure ·
Solid solution · Intermetallic compound · Carbide

✉ R. Liu
Rong.Liu@carleton.ca

1 Department of Mechanical and Aerospace Engineering, Carleton University, 1125 Colonel By Drive, Ottawa, ON K1S 5B6, Canada

2 Research Center of Laser Processing Technology and Engineering, Zhejiang University of Technology, Hangzhou, Zhejiang 310014, People's Republic of China

3 Kennametal Stellite Inc., 471 Dundas St E, Belleville, ON K8N 5C4, Canada

Introduction

Stellite alloys are cobalt-based superalloys, which display exceptional properties including high-temperature strength, wear/erosion, and corrosion/oxidation resistance. These alloys contain mainly alloying elements chromium (Cr) and tungsten (W) or molybdenum (Mo) as well as a small amount of carbon (C), in addition to cobalt (Co). The alloying behavior of many elements within Stellite alloys has been studied and they are known to provide a variety of behavior, as reported in the literature [1–15].

Stellite alloys can be generally grouped into two categories: CoCrW system and CoCrMo system. The main difference in Stellite alloy grade is C content, hence the amount and type of carbides formed in the alloys. Based on C content, Stellite alloys are classified as high-C alloys designed for wear service; low-C alloys for high-temperature service; and low-C alloys to combat corrosion or simultaneous corrosion and wear [1]. Although Stellite alloys have been extensively studied because of their wide and popular application, no sufficient investigation of the solidification behavior and associated microstructure of these alloys has been reported, in particular, relating these characteristics to their chemical composition. However, lack of this understanding has caused problems in industry where these materials are employed. For example, design of the sintering cycle for a powder metallurgy (PM) process or heating cycle for a heat treatment process of Stellite alloys requires information on phase transformation temperatures of the alloys during melting and solidification. For tribological applications, various wear modes involve different wear mechanisms. The microstructure and phases present determine the response of Stellite alloys to wear in different modes [16, 17]. Therefore, understanding these can help properly select Stellite alloys for designated

applications. To this end, ten Stellite alloys were selected to cover the two main categories with various C contents. They were studied with respect to phase transformation behavior in heating and cooling processes, and the microstructure with phases developed during solidification. The focus of this research was on the relations of chemical composition to solidification behavior and associated microstructure of Stellite alloys. The significance of this research is that the research outcomes can provide the material industry with technical guidance in the design, manufacturing, processing, heat treatment, improvement, and application of Stellite alloys.

Experimental

Ten Stellite alloys were selected from the CoCrW and CoCrMo systems; their chemical compositions are given in Table 1. These alloys are divided into three groups, as indicated in Table 1. Group A has four alloys from the CoCrW system, with W content varying between 4.5–32 wt% and high-C content in a range 1.2–2.4 wt%. Special attention should be paid to alloy A4; it contains very high-W content (32 wt%). The alloys in group B and group C are all from CoCrMo category, but the former has low-C content (<0.35 wt%) and the latter high-C content (>1.2 wt%).

For DSC analysis, the sample of each alloy was cut from cast products with a mass 20–30 mg. The maximum heating temperature was set to 1500 °C owing to the high melting point of Co. The samples were heated to 100 °C and held for a dwell time of 20 min, then continuously heated up to the ultimate temperature, held for 10 min, and finally cooled to room temperature. The heating and cooling rates were set at 10 °C/min. The phase transformation behavior of the material during heating and cooling processes was characterized by the DSC curve.

The solidified alloy samples from the DSC tests were then mounted by encapsulating into phenolic plastic compounds for microstructural analysis. The samples were metallographically prepared to a 1 μm alumina finish and electrolytically etched in a solution of 9 g CrO_3, 15 mL HCl, and 150 mL H_2O at 3 V for 10 s.

The microstructural analyses of the ten alloys were conducted on a scanning electron microscope (SEM) equipped with an energy dispersive spectroscopy (EDS) detector for elemental analysis and quantitative mapping. The phases in the microstructures were identified using the x-ray diffraction (XRD) with Cu Kα radiation.

Results

Microstructure and Phase

SEM images of solidified microstructure from the three groups of alloys are presented in Figs. 1, 2, 3. The common features in microstructure of these alloys are black and white phases uniformly distributed within a gray matrix. EDS was performed on each phase of these alloys to investigate their compositions and XRD was conducted on each of the alloys to identify the phases present.

For group A, the EDS spectra in Fig. 4 reveal that the gray phase is Co-rich, the black phase is Cr-rich, and the white phase is W-rich. The XRD patterns in Fig. 5 identify that the gray phase is face-centered cubic (fcc) Co solid solution and no hexagonal close-packed (hcp) phase is detected; the black phase is Cr_7C_3 carbide and the W-rich phase is $(Co,W)_6C$ carbide in alloy A2 and alloy A3, but no W-rich carbides are detected in alloy A1 due to the very small amount, instead two types of Cr-rich carbides, Cr_7C_3 and Cr_3C_2, are identified. In addition, although a small amount of B (1 wt%) is added to alloy A3, no B-containing phases are detected by the XRD analysis. This may be due to the resolution capacity of the XRD device used in this research, which is limited to detect phases in very small quantities. Different from the other three alloys in group A,

Table 1 Chemical compositions (wt%, Co in balance) of selected Stellite alloys

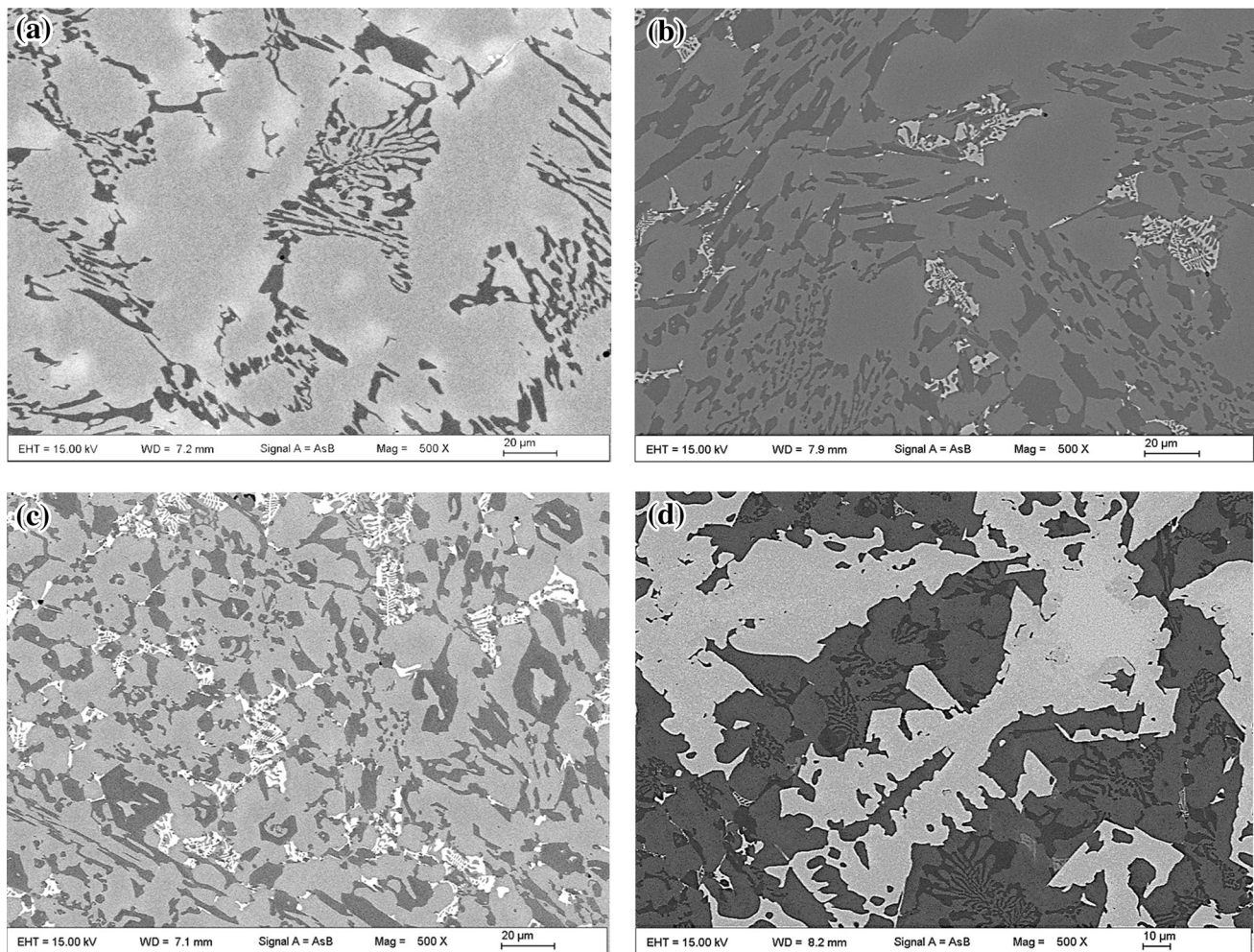| Alloy	Cr	W	Mo	C	Fe	Ni	Si	Mn	Others
Alloy A1	29	4.5	1.5	1.2	3	3	1.5	1	
Alloy A2	30	8.3		1.4	3	1.5	0.7	2.5	
Alloy A3	30.5	12.5		2.4	5	3.5	2	2	1B
Alloy A4	22	32		1.5					
Alloy B1	27		5.5	0.25	3	2.75	1	1	
Alloy B2	27		11	0.25	3	2.75	1	1	
Alloy B3	24		11.8	0.35	1	3.8	0.45	0.52	2.07Nb
Alloy C1	29		5	1.2	3	3	1.5	1.5	
Alloy C2	29		8.5	2	3	3	1.5	1.5	
Alloy C3	33		18	2.5	3	3	1.5	1.5	0.3B

Fig. 1 SEM microstructures at ×500: (**a**) alloy A1, (**b**) alloy A2, (**c**) alloy A3, and (**d**) alloy A4

alloy A4 contains a large volume fraction of white phase and minor black phase; the white phase is identified to be $(Co,W)_6C$ and Co_4W_2C carbides and the black phase is Cr_7C_3 carbide.

For group B, similar to group A, the gray phase is the Co solid solution matrix with the black and white phases embedded. However, the amounts of the black and white phases in alloy B1 are very small. Alloy B2 contains a small amount of black phase but large amounts of white phase. No black phase is observed in alloy B3. The EDS analyses found the black phase to be Cr-rich. The spectra in Fig. 6 show the white phase is Mo-rich and a small amount of Nb is also presented in the white phase of alloy B3. The XRD patterns in Fig. 7 indicate that the Co solid solution in these alloys is in fcc form, the black phase in alloy B1 and alloy B2 is $Cr_{23}C_6$ carbide, and the white phase is Co_3Mo intermetallic compound. NbC carbide is found in alloy B3 but this alloy does not have Cr-rich carbide. The reason for this is because of the presence of Nb, which has

stronger affinity to C than Cr [18], so that the small amount of C (0.35 wt%) in this alloy forms carbides easier with Nb than with Cr. Since the EDS analysis detects Nb present in the white phase, it is inferred that NbC carbide is mixed with the Co_3Mo intermetallic compound in the eutectic. The reason why this carbide phase is not observed in the SEM image of microstructure can be three: (1) NbC carbide is in the same color with Co_3Mo intermetallic compound in SEM image; (2) NbC carbide is in small quantities due to both low Nb and C contents in this alloy; and (3) NbC carbide may be tiny and dispersed within the Co_3Mo intermetallic compound.

For group C, the SEM image at ×500 (Fig. 3d) cannot display the entire microstructure of alloy C3 because the primary black phase in this alloy is very large in size but is distributed sparsely in the microstructure. Meanwhile, the eutectic phase in this alloy is too small to see in detail at low magnifications. Therefore, the lower magnification of ×100 and higher magnification of ×1500 were also used
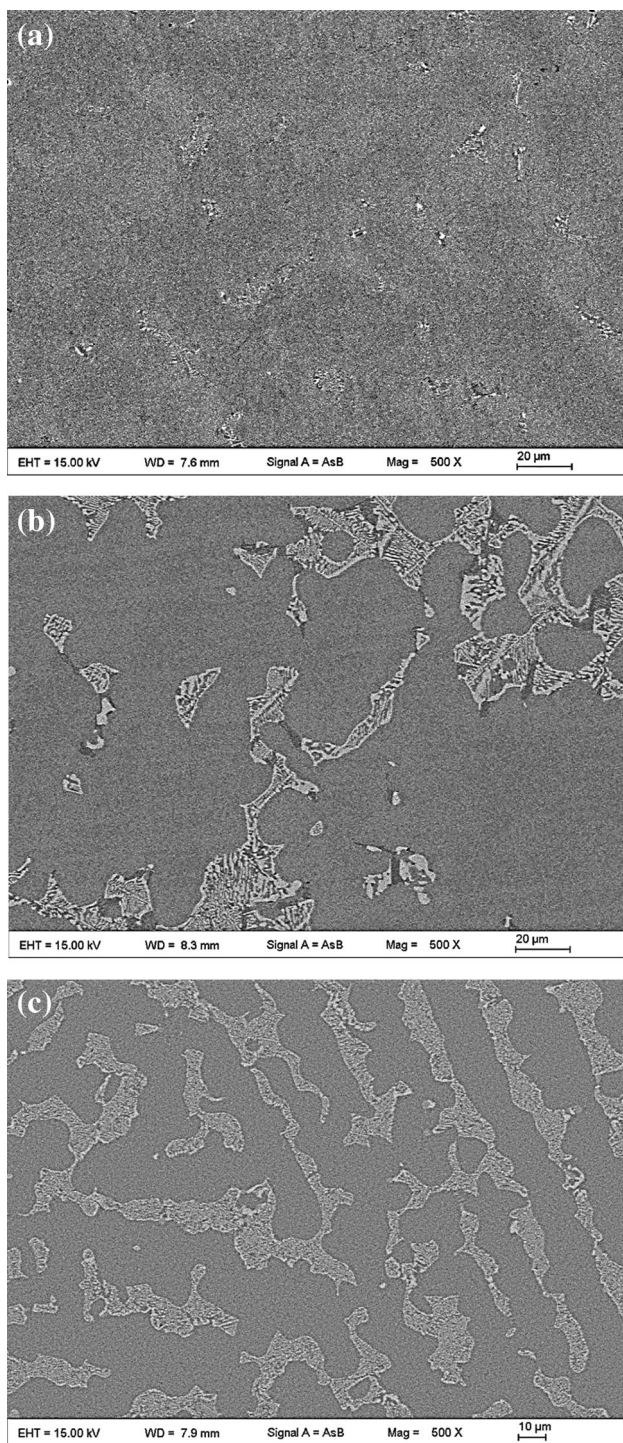
Fig. 2 SEM microstructures at ×500: (a) alloy B1, (b) alloy B2, and (c) alloy B3

for alloy C3. As observed in Fig. 3, Alloy C1 has large amounts of black phase and minor white phase embedded in the gray matrix, while alloy C2 has increased amounts of white phase and larger sizes of both black and white phases, compared with alloy C1. In the ×1500 image in

Fig. 3(e), alloy C3 has four distinct phases in black, white, gray, and light gray, respectively. The EDS analyses found that the black phase is Cr-rich; the spectra in Fig. 8 show that the white phase is Mo-rich and the light gray phase is also Cr-rich. The XRD analysis results reveal that the matrices of these alloys are fcc Co solid solution; the Cr-rich black phase of alloy C1 includes Cr_7C_3 and Cr_3C_2 carbides; the Cr-rich phase is Cr_7C_3 carbide and the white phase is $(Co,Mo)_3C$ carbide in alloy C2; and the Cr-rich phases in black and light gray of alloy C3 are all Cr_7C_3 and the white phase is $(Co,Mo)_3C$ (Fig. 9).

To quantify the carbides and intermetallic compounds in the alloys under study, the volume fractions of these components in these alloys were measured using SEM; the results are reported in Table 3. Alloy A4 has the largest volume fraction of carbides, followed by alloy C3. Alloy B1 has the least; the other two in this group also have less volume fractions of carbides and intermetallic compounds, compared with the other groups.

Phase Transformation Temperature

The phase transformation curves of the three groups of Stellite alloys were obtained from the DSC tests; but as examples, only the curves for one alloy from each group are presented in Fig. 10. These curves characterize the melting and solidification behavior of the alloys during heating and cooling, showing the phase transformation temperatures. For each alloy, the phase transformation curve comprises two parts: heating (melting) and cooling (solidification). Stellite alloys are multi-phase alloys, typically consisting of primary phase (either Co solid solution or carbides) and eutectic phase. Accordingly, on the phase transformation curves, generally there are two main exothermic peaks representing the two-phase transformations in both the heating and cooling processes, but segregation and secondary precipitation may occur in the alloys, which generate additional peaks on the curves; as seen in Fig. 10(c) for alloy C2, the first small peak on the cooling curve represents the segregation of the primary phase. However, for alloy B1, since the amounts of carbides and intermetallic compounds are very small, the eutectic phase solidification cannot be detected by the DSC analysis. As a result, on both the heating and the cooling curves, there is only one peak representing the melting and solidification of the solid solution, as shown in Fig. 10(b).

The critical data on the phase transformation curves include melting point, T_m, which is the temperature corresponding to the highest or strongest peak on the heating curve; primary phase solidification temperature, T_p, which is the temperature corresponding to the first large peak on the cooling curve (small peak represents segregation); eutectic phase solidification temperature, T_e, which is the
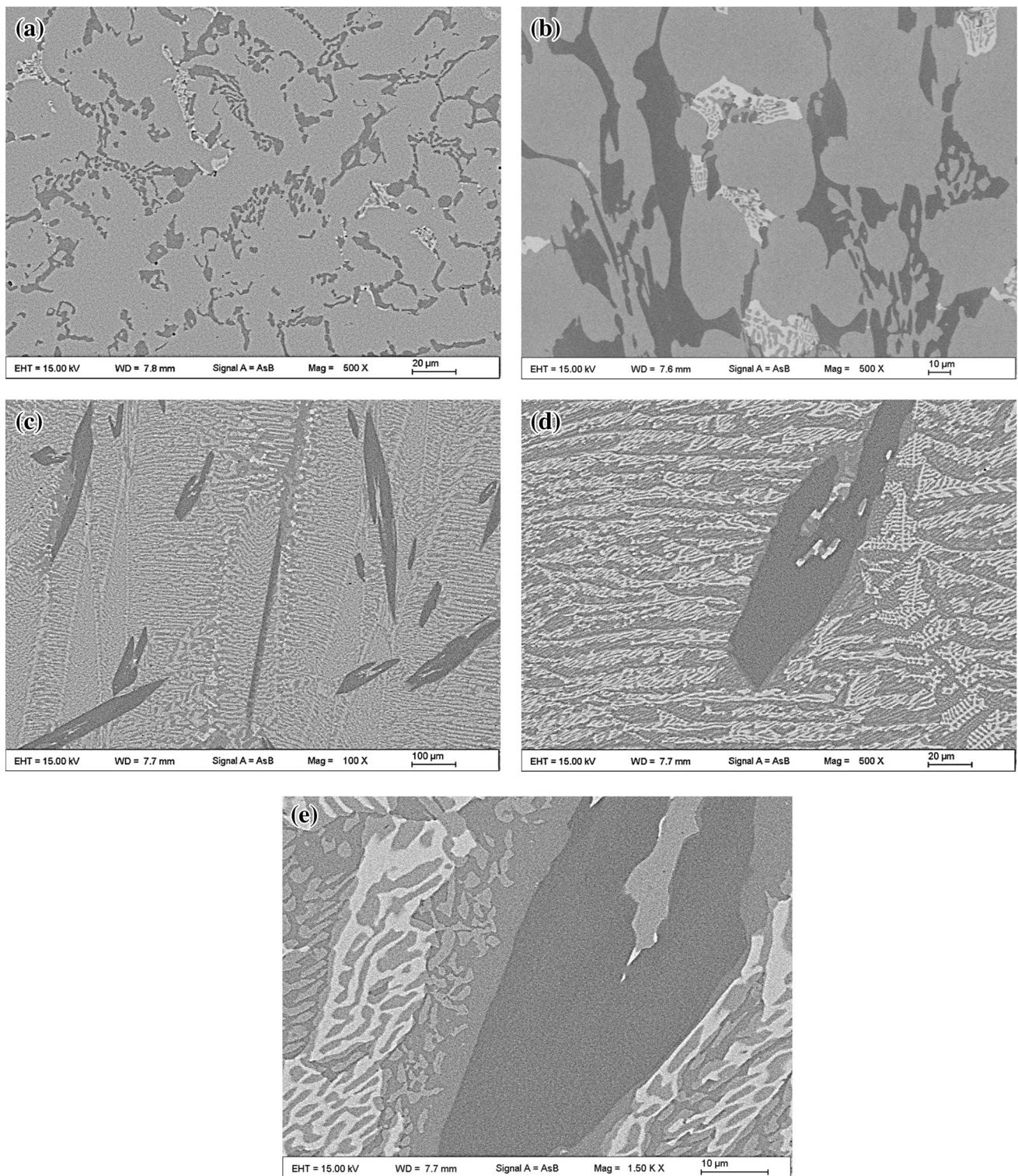
Fig. 3 SEM microstructures: (**a**) alloy C1 at ×500, (**b**) alloy C2 at ×500, (**c**) alloy C3 at ×100, (**d**) alloy C3 at ×500, and (**e**) alloy C3 at ×1500

temperature corresponding to the second large peak on the cooling curve (small peak represents segregation or secondary precipitation); and the solidification range, ΔT, which is the temperature range between the start of solidification (starting of the first peak) and the end of solidification (ending of the last peak) on the cooling curve.
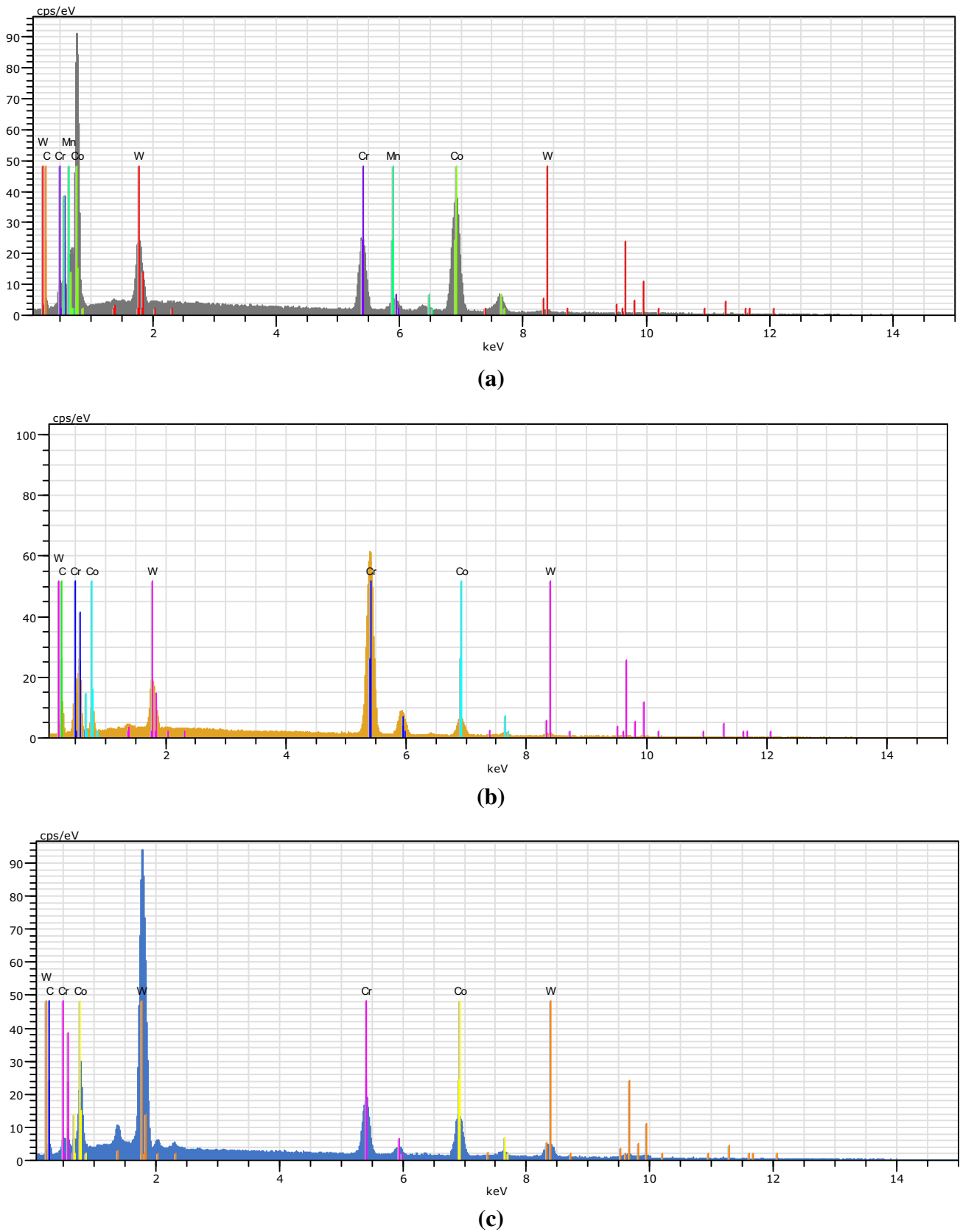
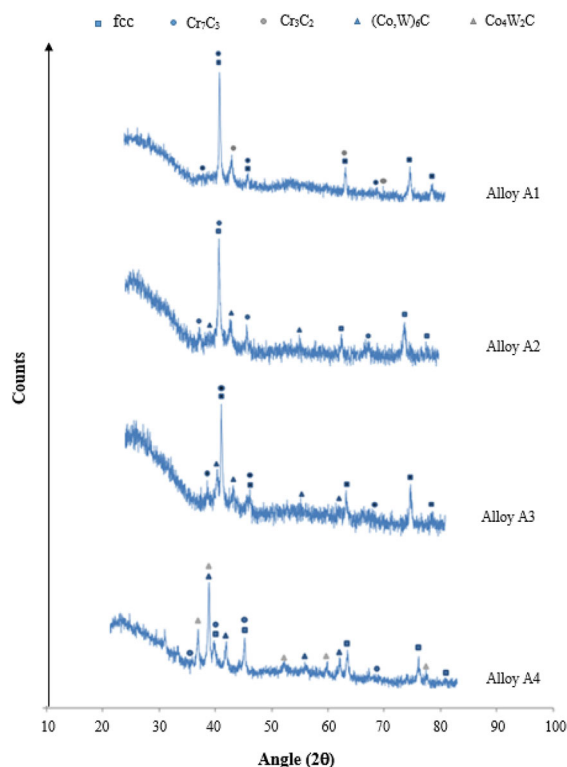Fig. 4 EDX spectra for the alloys of group A: (a) gray phase, (b) black phase, and (c) white phase

Fig. 5 XRD patterns for the alloys of group A

The critical phase transformation temperatures for the three groups of alloys are summarized in Table 2. It is shown that the alloys of group B, which contain low C, have higher melting point and higher primary phase solidification temperature than the alloys of the other groups, but this group of alloys has much smaller solidification ranges, compared with the other groups. However, there is no distinct difference in phase transformation behavior between group A and group C, which are both high-C Stellite alloys, although they are CoCrW system and CoCrMo system, respectively.

Discussion

Effects of Carbon

Carbon content in Stellite alloys governs the amount of carbides precipitated in the alloys, thus determining various properties of the alloys such as mechanical strength, high temperature, wear, and corrosion resistance, because carbides are the main strengthening agent of the alloys. Depending on C content, Stellite alloys may be hypoeutectic or hypereutectic. When C content is less than 2 wt%, the alloys are hypoeutectic; otherwise they are hypereutectic [2]. However, other alloying elements, such as W

and Mo, can change this convention [19, 20]. Among the alloys under investigation, alloy A3, alloy C2, and alloy C3 are hypereutectic, according to their C contents, with the Cr-rich carbides being the primary phase. However, alloy A4, although it has lower C content (1.5 wt%), is also hypereutectic, with the W-rich carbides being the primary phase, due to the very high-W content (32 wt%).

The carbide volume fractions of the alloys, reported in Table 3, demonstrate the carbon-dependence. It is evident that the carbide volume fraction is generally proportional to the C content. The alloys of group B contain very low-C content so that they have the least volume fractions of carbides. Alloy A3 and alloy C3 contain very high-C content; therefore, they have large volume fractions of carbides. However, due to the very high-W content, alloy A4 has larger volume fraction of carbides than alloy A3 and alloy C3, although it contains lower C content than the two alloys, because large amounts of W-rich carbides are precipitated in this alloy.

From DSC data in Table 2, hypoeutectic Stellite alloys generally have higher melting point than hypereutectic ones. The alloys of group B are all hypoeutectic; accordingly, they have higher melting point. Within group A, alloy A3 and alloy A4 are hypereutectic; consistently, they have lower melting point than the other alloys of the group. Similarly, among the alloys of group C, only alloy C1 is hypoeutectic and its melting point is higher than that of the other two alloys in the group. Besides, the low-C Stellite alloys, that is, the alloys of group B, have smaller solidification range. This may be due to less amounts of carbides and intermetallic compounds, which result in shorter time of the eutectic solidification during cooling.

Effects of Tungsten and Molybdenum

In addition to C, W and Mo also play an important role in the microstructure of Stellite alloys. In high-C Stellite alloys, high-W and Mo contents can induce W-rich carbides in CoCrW system and Mo-rich carbides in CoCrMo system. Furthermore, excessive W content can result in a hypereutectic alloy with lower C content, as demonstrated by alloy A4. It can be inferred that if the Mo content in High-C CoCrMo system is increased to a very high level ($\sim$32 wt%), similar to the W content in alloy A4, the primary phase of this alloy would be Mo-rich carbides, instead of Cr-rich carbides.

In low-C Stellite alloys, high-Mo content can generate Mo-rich intermetallic compounds, as observed on the alloys of group B. In high-C Stellite alloys, the amounts of W-rich and Mo-rich carbides increase with the W and Mo content in these alloys. This is due to W and Mo when present in small quantities, W and Mo in Stellite alloys exist in the solution matrix as solute atoms to provide
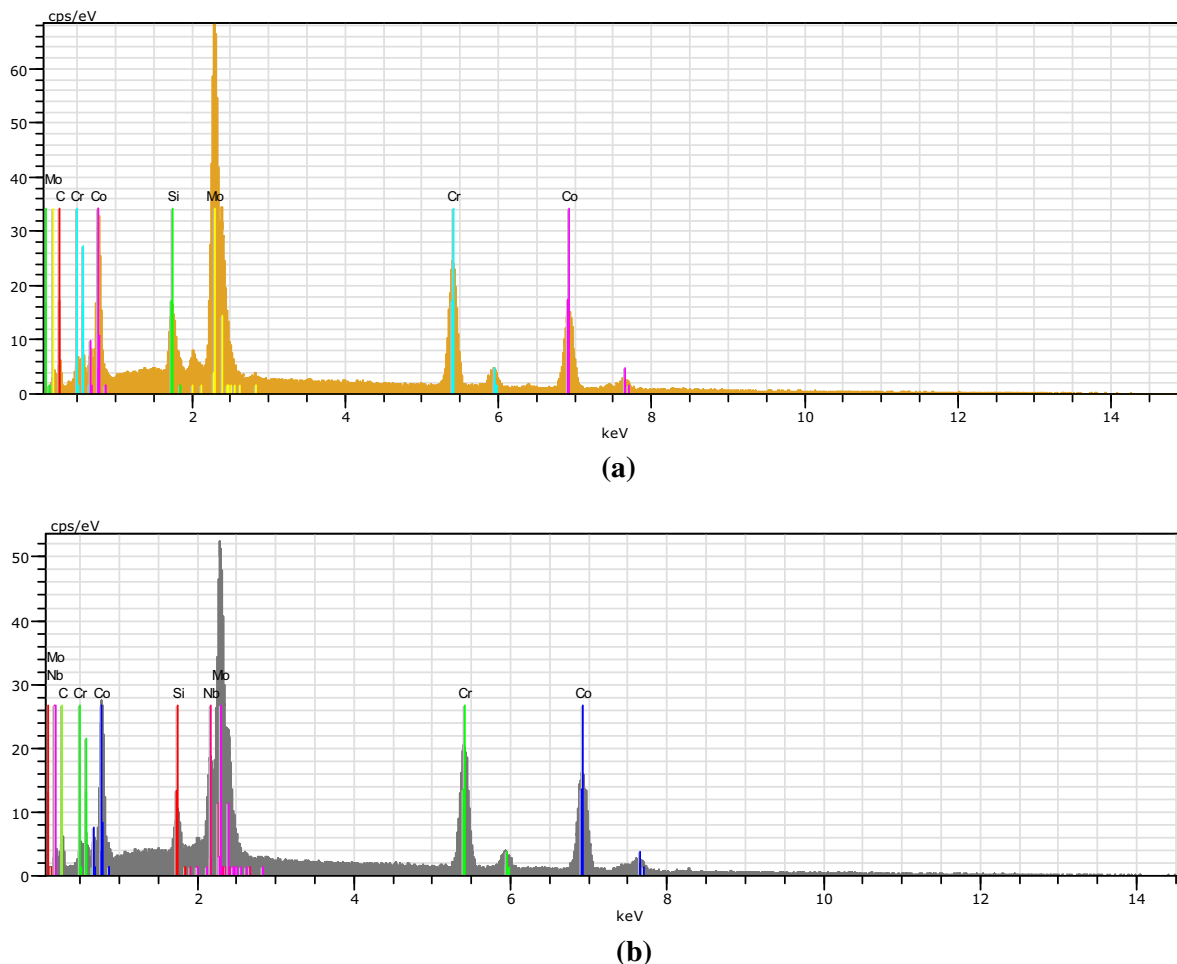
(a)

(b)

Fig. 6 EDX spectra for the alloys of group B: (**a**) white phase in alloy B1 and alloy B2 and (**b**) white phase in alloy B3
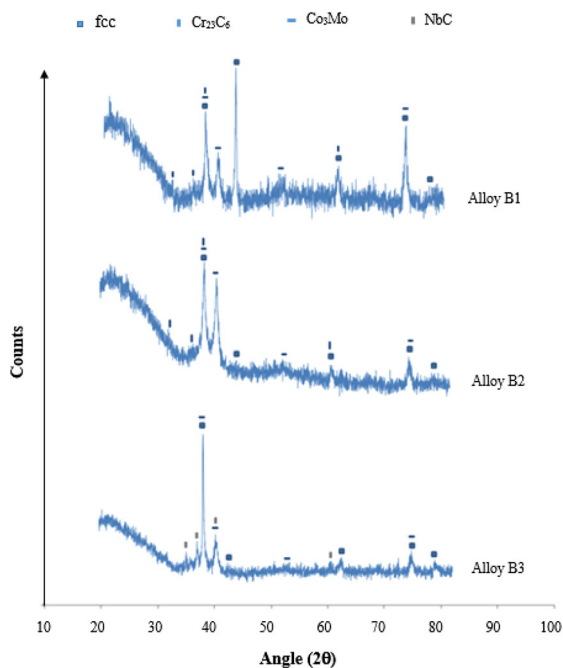

Fig. 7 XRD patterns for the alloys of group B

additional strength; but with the increase of their contents, the extra W and Mo form carbides with C. Due to high-C content, the higher the W and Mo contents, the more the amounts of the W-rich and Mo-rich carbides are formed in the alloys, since the solid solution matrix has been saturated with W and Mo and cannot take any more W and Mo.

Carbide Versus Intermetallic Compound

Carbides are the main strengthening agent of Stellite alloys; however, it is common to increase the wear resistance of these alloys by inducing intermetallic compounds. As demonstrated by the alloys of group B, adding more Mo in low-C Stellite alloys can generate Co_3Mo intermetallic compounds. To investigate if the intermetallic compound has similar effects to the carbides in Stellite alloys, the hardness of the selected alloys was measured using a Wilson Series 2000 Rockwell Hardness Tester; the average values are illustrated in Fig. 11. Linking the results in Table 3 with those in Fig. 11, it can be seen that the
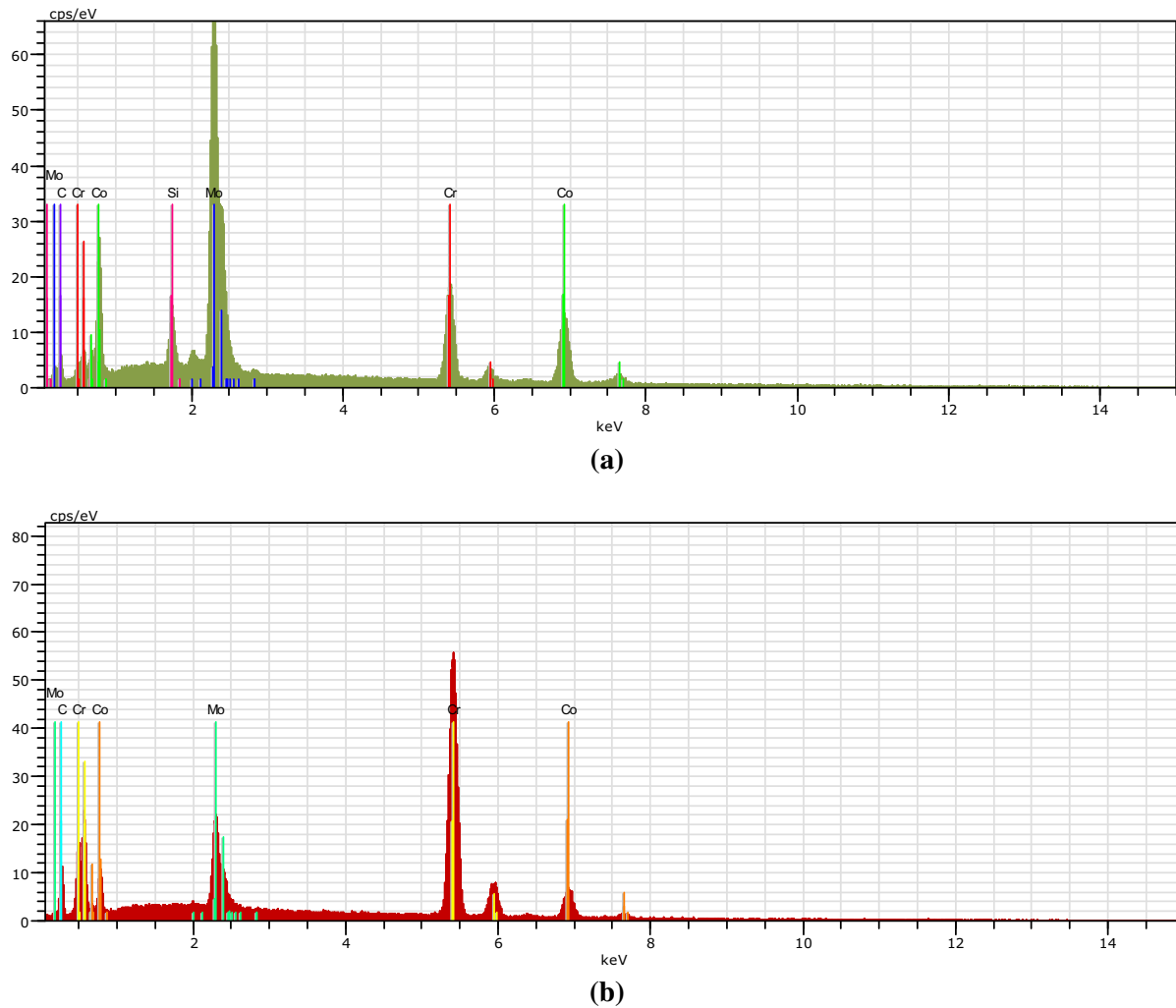
Fig. 8 EDX spectra for the alloys of group C: (a) white phase and (b) light gray phase in alloy C3
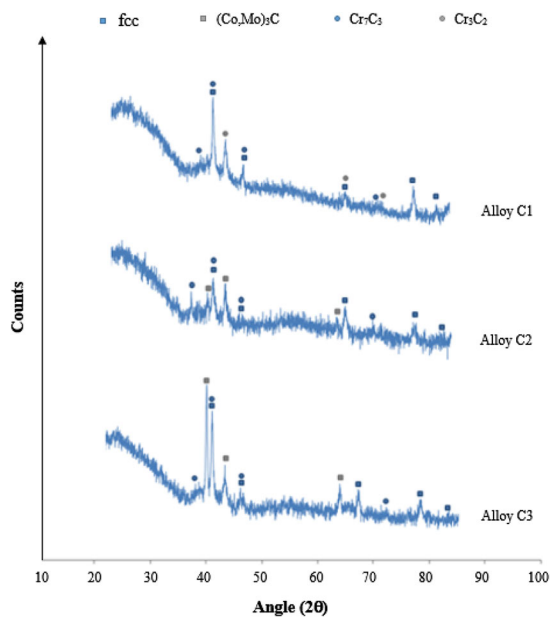

Fig. 9 XRD patterns for the alloys of group C

hardness of Stellite alloys increases with the volume fractions of carbides and intermetallic compound in the alloys. Attempts have been made to measure the hardness of various carbides in Stellite alloys such as Cr_7C_3 and $(Co,W)_6C$, and Co_3Mo intermetallic compound using the a microhardness tester. The hardness test data for Cr_7C_3 and $(Co,W)_6C$ are reliable, but not for Co_3Mo. This is due to the fact that the indentation can be made on single Cr_7C_3 and $(Co,W)_6C$ phases when they are the primary phase owing to the large size, like the primary Cr_7C_3 in alloy C3 and primary $(Co,W)_6C$ in alloy A4, but Co_3Mo is present in the eutectic phase of the alloys in group B, which is mixed with the carbide and Co solid solution; thus, the indentation made on Co_3Mo must cover other phases, resulting in inaccurate results. The average hardness values of Cr_7C_3 and $(Co,W)_6C$ obtained from the microhardness test are HV1404 and HV1356, respectively. Although the accurate hardness value of Co_3Mo cannot be obtained experimentally, the overall hardness results of alloy A1 and alloy B3

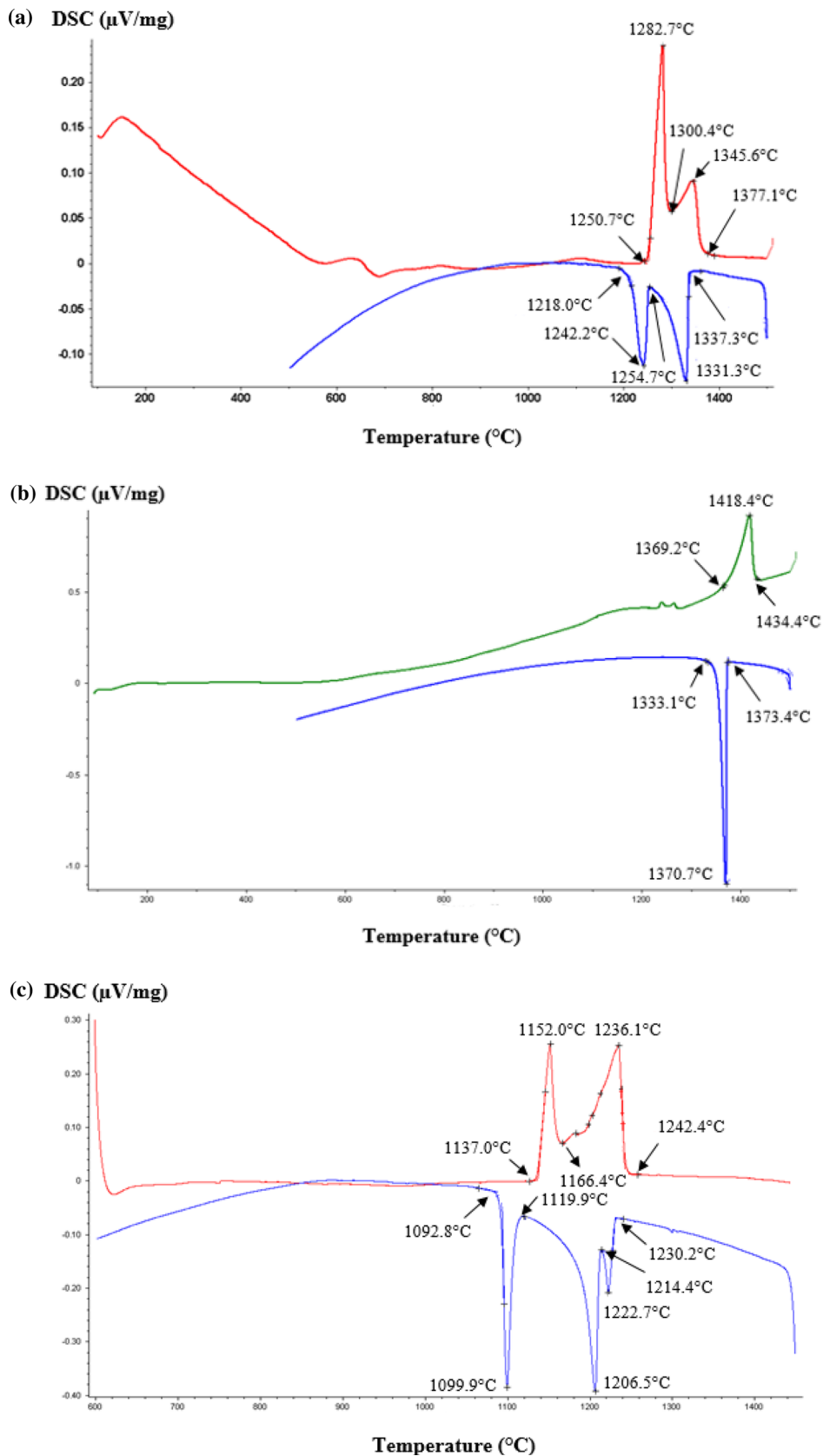**Fig. 10** Phase transformation curves: (**a**) alloy A1, (**b**) alloy B1, and (**c**) alloy C2

Table 2 Summary of DSC test data for selected Stellite alloy

Alloy	T_m (°C)	T_p (°C)	T_e (°C)	ΔT (°C)
Alloy A1	1282.7	1331.3	1242.2	119.3
Alloy A2	1292.3	1301.9	1236.3	113.4
Alloy A3	1267.5	1227.8	1127.7	147.6
Alloy A4	1250.4	1298.4	1166.6	193.0
Alloy B1	1418.4	1370.7		40.3
Alloy B2	1368.9	1379.6	1330.4	67.6
Alloy B3	1386.3	1320.6	1278.6	69.1
Alloy C1	1265.5	1311.0	1219.3	149.3
Alloy C2	1236.1	1206.5	1099.9	137.4
Alloy C3	1219.9	1215.1	1156.3	133.1

Table 3 Summary of volume fractions (%) of each phase in selected Stellite alloys

	W-rich or Mo-rich phase	Cr-rich phase	Co solid solution
Alloy A1	1.32	15.57	83.11
Alloy A2	3.55	22.77	73.68
Alloy A3	5.65	27.83	66.52
Alloy A4	43.54	11.64	44.82
Alloy B1	0.66	1.28	98.06
Alloy B2	8.92	2.49	88.59
Alloy B3	11.31	0	88.69
Alloy C1	2.64	13.91	83.45
Alloy C2	5.38	24.26	70.36
Alloy C3	19.6	25.09	55.31
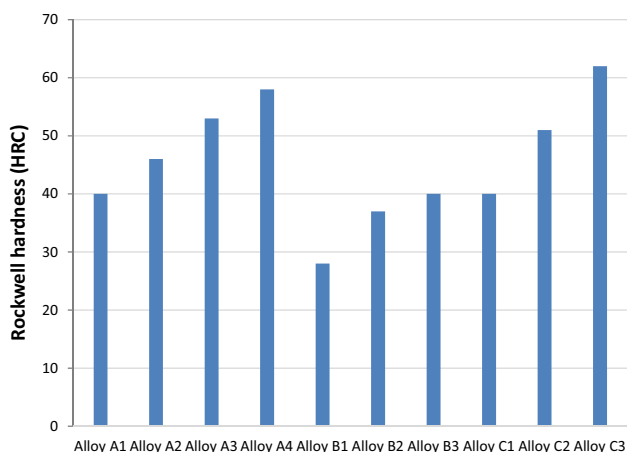
Fig. 11 Hardness of selected Stellite alloys

in Fig. 11 imply that Co_3Mo has comparable hardness to Cr_7C_3, because these two alloys have the same hardness and similar volume fraction of carbides or intermetallic compounds.

A reverse relationship between hardness and volume fraction of carbide/intermetallic compound is observed in alloy B2 and alloy B3. The former has slightly larger volume fraction of carbide/intermetallic compound, but it has lower hardness. This is not well understood because the white phase of alloy B3 contains minor NbC mixed with Co_3Mo, which cannot be identified and quantified, as discussed above. The authors hypothesize that (1) the quantities of Co_3Mo in these two alloys are not equal and/or (2) NbC and Cr_3C_2 have different hardnesses.

Conclusions

The typical microstructure of Stellite alloys consists of various carbides dispersed in a tough Co solid solution matrix. Carbon content is the key factor that determines the microstructure of these alloys. Depending on the C content, the alloy can be hypoeutectic (<2 wt% C) or hypereutectic (>2 wt%C). However, other alloying elements such as W and Mo also play an important role in the microstructure by forming W-rich and Mo-rich carbides.

Most carbides in Stellite alloys are Cr-rich, but when W and Mo are present in large quantities, they can induce W-rich and Mo-rich carbides in high-C Stellite alloys and Mo can generate Mo-rich intermetallic compound in low-C Stellite alloys. The Mo-rich intermetallic compound in low-C Stellite alloys has similar effects to the carbides in Stellite alloys on strengthening the alloys hardness.

The Stellite alloys with a hypoeutectic microstructure generally have higher melting point than those with a hypereutectic one; in other words, the Stellite alloys with larger volume fraction of carbides have lower melting point. Additionally, low-C Stellite alloys have smaller solidification temperature range than High-C ones.

References

1. J.R. Davis, *Nickel, Cobalt, and Their Alloys: Cobalt-Base Alloys* (ASM International, Materials Park, 2000)
2. W. Betteridge, *Cobalt and Its Alloys: Constitution and Metallography of Cobalt Alloys* (Halsted Press, Chichester, 1982)
3. A. Davin, D. Coutsouradis, Development of abrasion- and corrosion-resistant alloys for use in aqueous media. Cobalt **52**, 160–161 (1971)
4. S. Kapoor, R. Liu, X.J. Wu, M.X. Yao, Microstructure and wear resistance relations of Stellite alloys. Int. J. Adv. Mater. Sci. **4**(3), 231–248 (2013)
5. P. Huang, R. Liu, X.J. Wu, M.X. Yao, Effects of molybdenum content and heat treatment on mechanical and tribological

properties of a low-carbon Stellite alloy. J. Eng. Mater. Technol. **129**(4), 523–529 (2007)

6. C.T. Sims, A contemporary view of cobalt-base alloys. JOM **21**, 27–42 (1969)

7. K. Ando, T. Omori, J. Sato, Y. Sutou, K. Oikawa, R. Kainuma, K. Ishida, Effect of alloying elements on fcc/hcp martensitic transformation and shape memory properties in Co–Al alloys. Mater. Trans. **47**(9), 2381–2386 (2006)

8. M.C. Chaturvedi, Precipitation behavior of NbC in a CoNiCr alloy. Metallography **13**(2), 167–183 (1980)

9. A. Bauer, S. Neumeier, F. Pyczak, R.F. Singer, M. GÖken, Creep properties of different γ'-strengthened Co-base superalloys. Mater. Sci. Eng. A **550**, 333–341 (2012)

10. I. Campos, G. Ramirez, U. Figueroa, C. Velazquez, Paste bonding process: evaluation of boron mobility on borided steels. Surf. Eng. **23**(3), 216–222 (2007)

11. L.C. Wang, D.Y. Li, Effects of yttrium on microstructure, mechanical properties, high-temperature wear behavior of cast Stellite 6 alloy. Wear **255**(1–6), 535–544 (2003)

12. I. Radu, D.Y. Li, R. Llewellyn, Tribological behavior of Stellite 21 modified with yttrium. Wear **257**(11), 1154–1166 (2004)

13. I. Radu, D.Y. Li, The wear performance of yttrium-modified Stellite 712 at elevated temperatures. Tribo. Int. **40**(2), 254–265 (2007)

14. J.C. Shin, J.M. Doh, J.K. Yoon, D.Y. Lee, J.S. Kim, Effect of molybdenum on the microstructure and wear resistance of cobalt-base Stellite hardfacing alloys. Surf. Coat. Technol. **166**(2–3), 117–126 (2003)

15. M.X. Yao, J.B.C. Wu, W. Xu, R. Liu, Metallographic study and wear resistance of a high-C wrought Co-based alloy Stellite 706K. Mater. Sci. Eng. A **407**(1–2), 291–298 (2005)

16. S. Nsoesie, R. Liu, K.Y. Chen, M.X. Yao, Erosion resistance of Stellite alloys under solid-particle impact. J. Mater. Sci. Eng. B **3**(9), 555–566 (2013)

17. S. Nsoesie, R. Liu, K.Y. Chen, M.X. Yao, Analytical modeling of solid-particle erosion of Stellite alloys in combination with experimental investigation. Wear **309**(1–2), 226–232 (2014)

18. W.D. Callister Jr, D.G. Rethwisch, *Materials Science and Engineering—An Introduction: Atomic Structure and Interatomic Bonding* (Wiley, New York, 2010)

19. R. Liu, J.H. Yao, Q.L. Zhang, M.X. Yao, R. Collier, Sliding wear and solid-particle erosion resistance of a novel high-tungsten Stellite alloy. Wear **322–323**, 41–50 (2015)

20. R. Liu, X.J. Wu, S. Kapoor, M.X. Yao, R. Collier, Effects of temperature on the hardness and wear resistance of high-tungsten Stellite alloys. Metall. Mater. Trans. A **46**(2), 587–599 (2015)